PNAS NEXUS

PNAS Nexus, 2025, 4, pgaf047

https://doi.org/10.1093/pnasnexus/pgaf047
Advance access publication 10 February 2025
Research Report

Endometrial zinc transporter *Slc39a10/Zip10* is indispensable for progesterone responsiveness and successful pregnancy in mice

Yui Kawata[a,b], Jumpei Terakawa[b,c,*], Ayuu Takeshita[a], Takafumi Namiki[a,b,1], Atsuko Kageyama[a], Michiko Noguchi[b,d], Hironobu Murakami[b,e], Toshiyuki Fukada[f], Junya Ito[a,b,*] and Naomi Kashiwazaki[a,b]

[a]Laboratory of Animal Reproduction, School of Veterinary Medicine, Azabu University, 1-17-71 Fuchinobe, Chuo-ku, Sagamihara 252-5201, Japan
[b]Graduate School of Veterinary Science, Azabu University, 1-17-71 Fuchinobe, Chuo-ku, Sagamihara 252-5201, Japan
[c]Laboratory of Toxicology, School of Veterinary Medicine, Azabu University, 1-17-71 Fuchinobe, Chuo-ku, Sagamihara 252-5201, Japan
[d]Laboratory of Theriogenology, School of Veterinary Medicine, Azabu University, 1-17-71 Fuchinobe, Chuo-ku, Sagamihara 252-5201, Japan
[e]Laboratory of Infectious Diseases, School of Veterinary Medicine, Azabu University, 1-17-71 Fuchinobe, Chuo-ku, Sagamihara 252-5201, Japan
[f]Laboratory of Molecular and Cellular Physiology, Faculty of Pharmaceutical Sciences, Tokushima Bunri University, 180 Nishihamahouji, Yamashirocho, Tokushima-City, Tokushima 770-8514, Japan
*To whom correspondence should be addressed: Email: terakawa@azabu-u.ac.jp (J.T.), Email: itoj@azabu-u.ac.jp (J.I.)
[1]Present address: Department of Life Science Frontiers, Center for iPS Cell Research and Application (CiRA), Kyoto University, 53 Kawahara-cho, Shogoin, Sakyo-ku Kyoto 606-8507, Japan.
Edited By David Brenner

Abstract

Zinc is a critical trace element that is important for various biological functions including male and female reproductive systems, but the molecular mechanisms that underlie fertility have been unclear. We show here that zinc signaling in the endometrial tissue is indispensable for successful pregnancy in mice. We observed that a uterine-specific genetic deletion of *Slc39a10/Zip10*, which encodes one of the zinc transporters to elevate the cytoplasmic level of zinc, results in female infertility due to failure of embryo invasion into the endometrium and subsequent embryonic loss. *Zip10* mRNA is expressed in uterine tissues, especially in the decidualizing stromal cells during embryo implantation. The absence of ZIP10 leads to attenuation of progesterone–progesterone receptor (PGR) signals between the epithelium and the stroma, including abnormal expression of the PGR and its target molecules in both the epithelium and stroma in vivo. We found that depletion of intracytoplasmic zinc ions due to loss of ZIP10 disrupts the change in nuclear-to-cytoplasmic localization of GLI1, which is critical for PGR signaling in the decidualizing stromal cells in vitro not only in mice but also in humans. Our findings (i) highlight a biological relevance of ZIP10-mediated zinc homeostatic regulation in the establishment of a successful pregnancy and (ii) will help to prevent infertility in humans.

Keywords: Slc39a/Zip10, embryo implantation, zinc homeostasis, progesterone receptor signaling, GLI1

Significance Statement

As zinc homeostasis has a great impact on reproductive outcomes, zinc signaling is suspected to play one or more important roles in the establishment and maintenance of pregnancy, but the details remain elusive. In the present study, we found that inhibition of zinc signaling by deficiency of the endometrial zinc transporter ZIP10 leads to attenuation of progesterone receptor signaling, resulting in failure of embryonic invasion, and subsequent embryonic loss. Zinc homeostasis in uterine stromal cells is important for changes in the cytoplasmic-nuclear localization of GLI1, which is critical for progesterone receptor signaling, and thus for the differentiation and proliferation of normal endometrial cells.

Introduction

Infertility, defined as the failure to achieve pregnancy after 12 months of regular unprotected sexual intercourse (1), is a global problem affecting an estimated 186 million of people of reproductive age worldwide (2). The causes of infertility include male factor (30%), female factor (35%), and combined factor (20%); 15% of infertility cases remain unexplained (3). Growing evidence suggests that parental nutritional status affects both fertility and the offspring's development and health (3, 4). Nutrients such as folic acid, vitamins, and minerals, are important for both male and female reproduction, but the nutrient-associated mechanisms that underlie fertility have not been determined (5).

Competing Interest: The authors declare no competing interests.
Received: January 15, 2024. **Accepted:** January 21, 2025

Zinc is an essential trace mineral that is involved in the regulation of gene expressions and protein synthesis by affecting >300 enzyme activities (6, 7). Adult humans have approx. 2–3 g of zinc in their bodies and require a zinc intake of 8 and 11 mg/day for females and males, respectively (8). Zinc deficiency and elevated intracellular zinc levels have a great effect on several biological processes involving the nervous, immune, and reproductive systems (7, 9, 10). Zinc deficiency during pregnancy in humans has a significant impact on maternal health and fetal and neonatal development (11–13). The deficiency in males also has been reported to cause impaired gonadal development and dysfunction (14). In mice, experimental zinc deficiency causes infertility, delayed fetal growth, fetal death and malformations, and delayed sexual maturation (15–17).

Zinc has only one valence state as the zinc ion, Zn (II), which interacts with many molecules in biological processes (18–20). Zinc signaling is the action of zinc ions as intracellular and extracellular signaling factors mediated by zinc-related proteins, such as zinc-finger proteins. The human body's intracellular zinc level is tightly regulated by zinc transporters, which include two of the solute carrier protein families: SLC30A (zinc transporter, ZnT) and SLC39A (Zrt-, Irt-related protein, ZIP) (21). ZnT transports zinc ions from the cytoplasm to the extracellular and intracellular organelles, whereas ZIP transports zinc ions from the extracellular and intracellular organelles to the cytoplasm (22, 23). In mammals, nine types of ZnT (ZnT1 to ZnT9) and 14 types of ZIP (ZIP1 to ZIP14) have been identified (21, 24). These zinc transporters are expressed in a tissue- and cell-specific manner and have different physiological roles (21, 25, 26). As zinc homeostasis has a great impact on reproductive outcomes, zinc transporters are suspected to play one or more important roles in the establishment and maintenance of pregnancy through the regulation of zinc dynamics, but the details remain elusive.

In this study, we focused on SLC39A10/ZIP10, which localizes to the cell membrane and is responsible for the influx of zinc ions into the cytoplasm (27). It has been reported that ZIP10 plays an important role in regulating homeostasis and functions of B lymphocytes (28, 29), suggesting that ZIP10 is necessary for B cell-mediated acquired immunity. ZIP10 also plays an important role in intracellular zinc homeostasis and is critical for hematopoietic stem cell survival (30). As demonstrated by the data in the gene annotation portal bioGPS (http://biogps.org/) (31), *ZIP10* expression is relatively high in the human and mouse uterus and placenta. To clarify the role of ZIP10 during pregnancy, we have generated uterine-specific *Zip10*-deficient mice, and we observed that these females are mostly infertile. Our findings help clarify the precise mechanism of infertility caused by lack of *Zip10* in the endometrium.

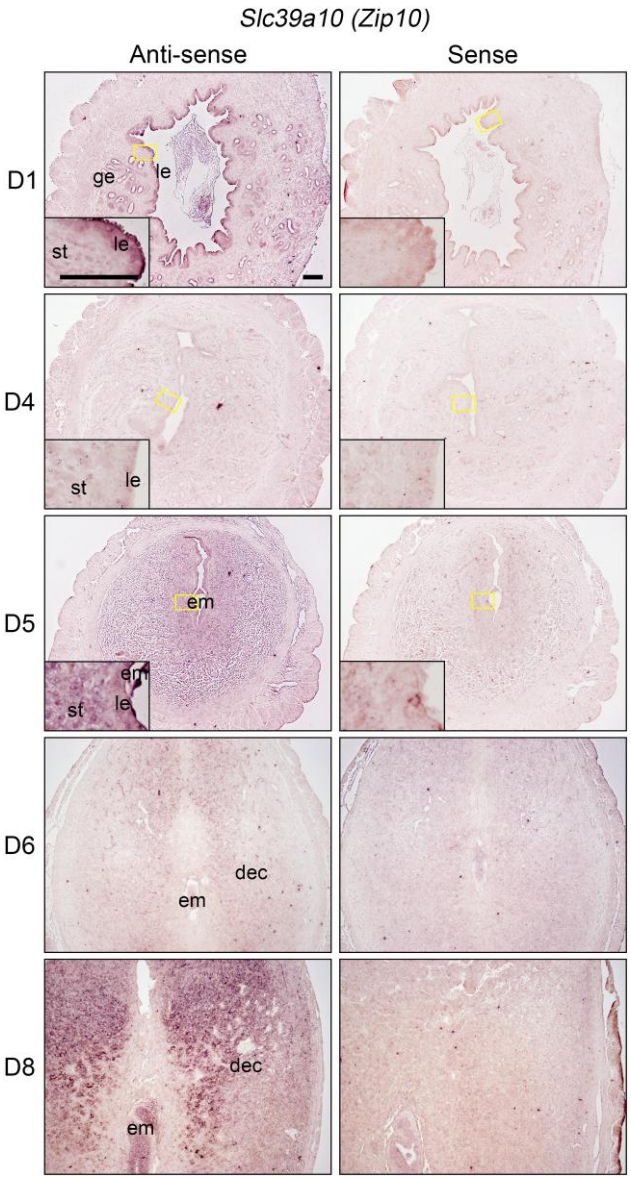

Fig. 1. Spatiotemporal expression of *Slc39a10/Zip10* mRNA in the pregnant mouse uterus. Signals (dark purple) were detected by an antisense probe (left). The sense probe (right) shows the background signal. *Slc39a10/Zip10* mRNA was detectable in the luminal and glandular epithelium at day 1 of pregnancy (D1), in differentiating stromal cells at D5, and in decidual cells at D8. Scale bar: 100 μm. dec, decidua; em, embryo; ge, glandular epithelium; le, luminal epithelium; st, stroma.

Results

Zip10 expression in the pregnant mouse uterus

We first examined the *Zip10* expression in the pregnant mouse uterus. *Zip10* mRNA expression was detected in the uterine epithelium at the first day (D1) of pregnancy (Fig. 1). A relatively strong expression of *Zip10* in stromal cells was observed on D5, when the embryos undergo an attachment reaction to the luminal epithelium. Stromal expression of *Zip10* was observed in decidualizing stromal cells, and secondary decidualized cells were clearly positive for *Zip10* on D8 as shown in Fig. 1.

Pregnancy failure of the uterine-specific *Zip10*-deficient females

To determine whether the deletion of the *Zip10* gene in the uterine tissue affected the pregnancy outcomes in the mice, we generated uterine-specific *Zip10*-deficient mice (*Zip10* cKO) driven by Pgr^{Cre}, which targets directed recombination in the female reproductive tracts (32, 33) (Fig. S1). We confirmed the loss of ZIP10 expression in the *Zip10* cKO endometrium (Fig. S2). We crossed the control and *Zip10* cKO females with sexually mature wildtype males. Control females ($n = 11$) gave birth to an average of 6.8 ± 0.5 pups, whereas only five out of the 23 *Zip10* cKO females gave birth; they produced a total of 13 pups (Fig. 2A). The average number of pups produced by the *Zip10* cKO females was 0.6 ± 0.3 (Fig. 2A), demonstrating that the *Zip10* cKO mice were predominantly infertile. We then examined the pregnant uteri on D5, D6, D8, and D10 to determine when pregnancy failure occurred (Fig. 2B).

On D5, the blue dye injections visualized the implantation sites in *Zip10* cKO mice as well as the control mice, suggesting the number of implantation sites was comparable between the control and

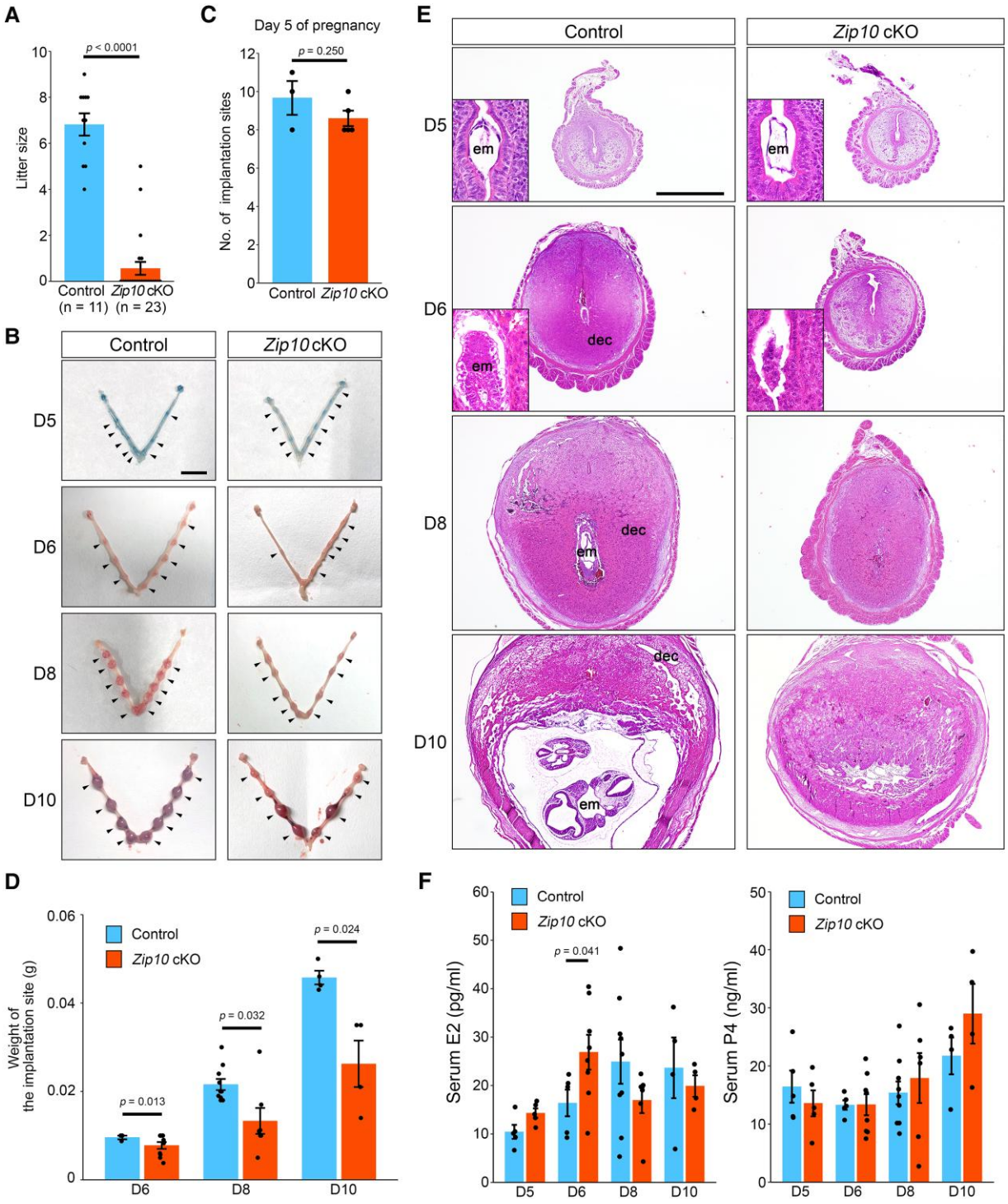

Fig. 2. Failure of pregnancy maintenance in uterine-specific *Slc39a10/Zip10*-deficient females. A) Pregnancy outcomes from control and *Zip10* cKO females. B) Representative uteri from control and *Zip10* cKO females from D5 to D10. Implantation sites are shown by arrowheads (visualized by a blue dye injection) on D5. Scale bar: 1 cm. C) The number of implantation sites were comparable between the control and *Zip10* cKO females on D5. D) The average wet weight of each implantation site was significantly reduced in the *Zip10* cKO mice on D6, D8, and D10. E) Representative images of uterine cross-sections stained by H&E. Scale bar: 1 mm. dec, decidua; em, embyo. F) Serum levels of 17β-estradiol (E2) and progesterone (P4) from D5 to D10.

Zip10 cKO groups (Fig. 2B, C). From D6 to D10 however, the wet weight of each implantation site became significantly lower in the *Zip10* cKO females compared with the control females (Fig. 2D). Histological observations revealed that on D5, (i) embryos were positioned at the antimesometrial side of the slit-like uterine lumen, and (ii) no apparent difference in the positions between the *Zip10* cKO and control groups (Fig. 2E). Nevertheless, on D6 the uterine lumen was not closed and decidualization was not sufficiently induced in the *Zip10* cKO females, with the result that embryos did not invade the endometrium (Fig. 2E). In the *Zip10* cKO females, embryonic loss was observed as early as D8, and most of the embryos were regressed and resorbed by D10 (Fig. 2B, E).

Since both 17β-estradiol (E2) and progesterone (P4) are required to induce embryo implantation and optimal decidualization, we

measured the serum E2 and P4 levels in control and *Zip10* cKO females. On D6 of pregnancy, the E2 levels were higher in the *Zip10* cKO females compared with the control females, whereas the P4 levels were comparable between the control and *Zip10* cKO females (Fig. 2F). No significant difference was observed in ovarian morphology; both groups of females developed multiple corpus lutea (Fig. S3). To test the possibility that higher E2 levels affect the pregnancy outcome in *Zip10* cKO females, we performed ovariectomies and exogenous E2 and P4 administrations to control the hormone levels and timing of embryo implantation (Fig. S4A). The experimental procedure in this study induced a one-day delay in the embryo implantation and decidualization process. The control females exhibited the successful embryo implantation and decidualization, but the *Zip10* cKO females failed to undergo optimal decidualization despite the control of the hormone levels (Fig. S4B, C). These results suggest that the embryonic loss in *Zip10* cKO females is mainly due to the functional defect of the endometrium, which is histologically manifested by D6 of pregnancy.

To know whether the loss of *Zip10* causes a fundamental loss of endometrial function, we performed RNA sequencing between the control and *Zip10* cKO uterus on D4, just before embryo implantation (Fig. S5, Datasets S1). In total, only 44 genes were differentially expressed between the *Zip10* cKO and control. Although several genes related to lymphocyte- and leukocyte-mediated immunity, and fibroblast growth factor 2 (*Fgf2*) were upregulated in the *Zip10* cKO uterus, but no other critical factors associated with uterine function and embryo implantation were observed, suggesting that the genetic defect of *Zip10* does not affect the phenotype before embryo implantation.

Abnormal PGR expression in the *Zip10* cKO uterine epithelium

To further investigate the pregnancy failure in *Zip10* cKO females, we performed an immunofluorescence evaluation for the epithelial marker CDH1 (also known as E-cadherin), in the uterine tissue during embryo implantation (Fig. 3A). In the controls, luminal epithelial cells were removed from D5 to D6, and embryos were placed directly in contact with decidualized stromal cells (Fig. 3A). In contrast, we observed on D6 that in the *Zip10* cKO females the luminal epithelial cells had remained intact (Fig. 3A). Since the cessation of luminal epithelial cell proliferation is essential for embryo implantation and since aberrant epithelial proliferation blocks the embryo implantation process (34), we examined the cell proliferation status by performing MKI67 staining on D5 (Fig. 3B). MKI67-positive cells were not found in the epithelium of either the control or *Zip10* cKO. On the other hand, the proliferation of subluminal stromal cells was increased in the *Zip10* cKO compared with the control groups (Fig. 3B, C). We confirmed that PTGS2 (also known as COX2) expression was found in the luminal epithelium and subluminal stromal cells in both the control and *Zip10* cKO, suggesting the initial interaction between embryo and endometrium (Fig. 3D).

We further examined the expression of estrogen receptor alpha (ERα, ESR1) and PGR by IHC during early pregnancy (Fig. 3E, F). No remarkable difference in ERα expression was observed on D5 (Fig. 3E). PGR expression was switched from the luminal epithelium to the stroma in the controls from D4 to D5, but PGR was continuously expressed in the luminal epithelium in the *Zip10* cKO group on D5 (Fig. 3F, G). The results of the qPCR analysis confirmed that the overall expression of *Pgr* mRNA was decreased in the *Zip10* cKO group on D5, which is consistent with the weak expression of PGR in stromal cells (Fig. 3F–H). Not only *Esr1* mRNA but also the expressions of leukemia inhibitory factor (*Lif*), a key regulator of embryo attachment (35) and its receptor, *Lifr,* were not significantly different between the control and *Zip10* cKO groups on D5 (Fig. 3H). These results suggest that PGR signaling appears to be disrupted in *Zip10* cKO mice, leading to the prevention of on-time embryo implantation.

Defects of PGR signaling in the *Zip10* cKO uterus

Since PGR expression was abnormally sustained in the luminal epithelium in the *Zip10* cKO group during the embryo implantation process, we investigated the expression of downstream targets of PGR. The results demonstrated that preceded by small implantation sites in *Zip10* cKO at D6, the expression of well-known genes related to the decidualization, including *Hoxa10*, *Bmp2*, and *Wnt4* (36, 37) were significantly decreased in the *Zip10* cKO uteri compared with the control uteri on D5 (Fig. 4A). Indian hedgehog (*Ihh*), which is expressed in the uterine epithelium under the control of PGR (38), was significantly upregulated in the *Zip10* cKO group compared with the controls (Fig. 4A). Activated IHH acts on patched receptor 1 (*Ptch1*) in neighboring cells to remove smoothened (*Smo*) inhibition, activating the glioma-associated oncogene homolog 1 (*Gli1*) and inducing factors such as chicken ovalbumin upstream promoter transcription factor II (COUP-TFII, encoded by *Nr2f2*) (39).

Intriguingly, the expressions of *Gli1* and *Nr2f2* mRNA were significantly decreased on D5 in *Zip10* cKO group compared with the controls (Fig. 4A). These results were further confirmed by the immunostaining; the expressions of SMO, GLI1, and COUP-TFII were markedly decreased in the pregnant uteri of *Zip10* cKO mice, especially in the stroma (Fig. 4B, Fig. S6). The expression of a stromal PGR-regulated factor, i.e. heart and neural crest derivatives expressed 2 (*Hand2*) (34) was also downregulated in the *Zip10* cKO uteri (Fig. 4A). Taken together, these results indicated that PGR signaling was disrupted in the *Zip10* cKO mice.

It has been demonstrated that epithelial PGR stability is controlled by the transcription factor, forkhead box O1 (FOXO1), based on the observation that FOXO1 ablation resulted in an increase in PGR signaling, as PGR expression was retained in the uterine epithelium during the window of receptivity (40). We therefore analyzed the expression of FOXO1 and found that it was expressed in the uterine epithelium of both the control and *Zip10* cKO mice (Fig. 4C). Although FOXO1 was not a primary target of ZIP10 deficiency, however, fewer FOXO1-positive cells were found in the peri-embryonic epithelial cells in the control, whereas more positive cells were found in the *Zip10* cKO (Fig. 4C, D). This suggests that FOXO1 may be involved in the persistent expression of PGR expression in *Zip10* cKO.

We also detected the expression of *Epas1* (also known as hypoxia-inducible factor 2 alpha [*Hif2α*]), which is expressed in the subepithelial stroma and regulates embryo invasion (41, 42). The expression of *Epas1* was comparable between the control and *Zip10* cKO uteri on D6 (Fig. S7).

Zinc depletion and decidualization in *Zip10* cKO uterine stromal cells

We next investigated whether decidualization is inducible in the *Zip10* cKO uterine stroma. Interestingly, decidualization was partially induced by intrauterine infusion of sesame oil in *Zip10* cKO mice, whereas gross uterine weight was significantly lower than control (Fig. 5A, B). No significant difference was observed in the expression of decidualization marker genes in the reacted regions between the control and *Zip10* cKO (Fig. S8). We thus isolated

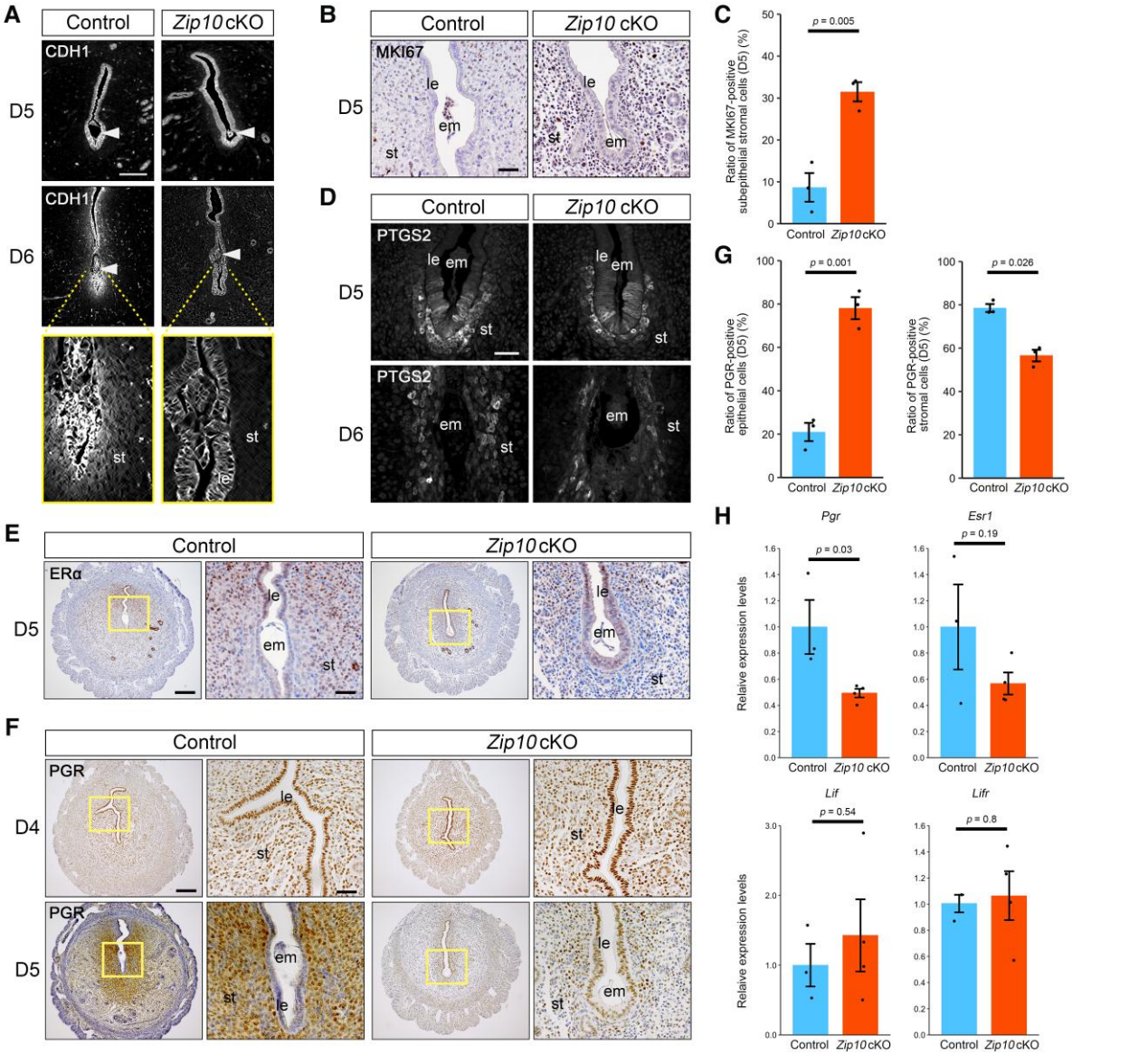

Fig. 3. Extraction of luminal epithelial cells surrounding the embryo was not induced in *Zip10* cKO mice. A) Immunofluorescence of CDH1 in sections of implantation sites on D5 and D6. The embryo (*arrowheads*) directly contacts the subepithelial stroma in the controls on D6, but not in the *Zip10* cKO mice. Scale bar: 200 μm. le, luminal epithelium; st, stroma. B) Immunostaining for MKI67. Scale bar: 50 μm. em, embryo; le, luminal epithelium; st, stroma. No MKI67-positive epithelial cells were observed in either the control or the *Zip10* cKO mice, but more positive cells were found in the stroma in *Zip10* cKO (C). D) Immunofluorescence of PTGS2 (COX2). Scale bar: 50 μm. em, embryo; le, luminal epithelium; st, stroma. E, F) Immunostaining for ERα (E) and PGR (F). Epithelial PGR expression was low in the controls on D5 but was sustained in the *Zip10* cKO mice, whereas stromal PGR expression was lower in *Zip10* cKO compared with the control (G). Scale bars: 50 μm (right panels) and 200 μm (left panels). em, embryo; le, luminal epithelium; st, stroma. H) Relative mRNA expression of *Pgr*, *Esr1*, and the implantation-related factors *Lif* and *Lifr*.

stromal cells from both control and *Zip10* cKO mice on D4 and performed in vitro decidualization using E2 and P4 (37) (Fig. 5C). The results demonstrated that decidualization can be induced by isolated primary stromal cells from *Zip10* cKO mice as well as control mice by assessing positive ALP staining (Fig. 5D), suggesting that stromal cells have the ability to differentiate.

To address whether the deletion of *Zip10* led to intracellular zinc depletion, we examined the intracellular zinc level by using a zinc ion indicator, FluoZin-3AM. FluoZin-3AM fluorescence was detected in the stromal cells of control females, but not those of *Zip10* cKO females (Fig. 5E). We confirmed that ZIP10 was absent in *Zip10* cKO stromal cells (Fig. 5F). We also observed the clear differentiation of GLI1 protein localization between the control and *Zip10* cKO stromal cells; GLI1 was detectable in the nucleus by 24 h after decidual stimuli (E2 + P4) in both control and *Zip10* cKO cells (Fig. 5F, G). At 72 h after decidual stimuli, GLI1 was localized in the cytoplasm in the control cells but in the nucleus in *Zip10* cKO cells (Fig. 5F, G), supporting the concept that GLI1 localization and P4 signaling are regulated by the intracellular zinc levels. We further tested whether zinc supplementation could improve GLI1 localization in *Zip10* cKO stromal cells (Fig. 5H). We found that chloroquine treatment shifted GLI1 localization from the nucleus to the cytoplasm in parallel with increased intracellular zinc levels (Fig. 5H).

We further tested whether ZIP10 function is conserved in human uterine stromal cells by shRNA-based ZIP10 knockdown. We found that transfection with Zip10-sh induced depletion of cytosolic zinc ions in a large number of cells (Fig. 6A).

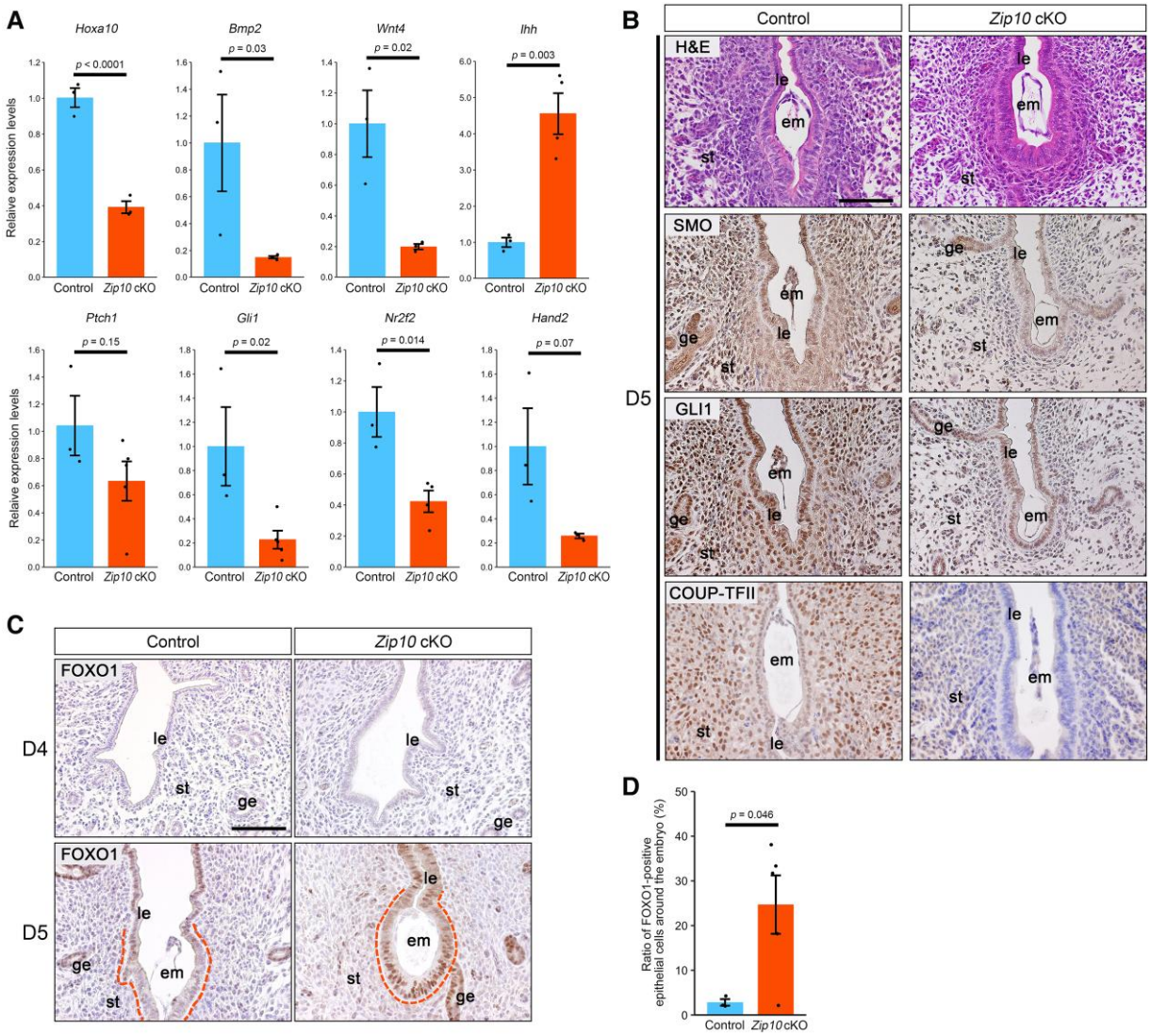

Fig. 4. P4-PGR target genes are disrupted in *Zip10* cKO mice. A) Relative mRNA expressions of decidual marker genes and P4-PGR target genes. B) H&E staining and immunostaining for SMO, GLI1, and COUP-TFII. These expressions were reduced in the *Zip10* cKO uteri compared with the controls. Scale bar: 100 μm. em, embryo; ge, glandular epithelium; le, luminal epithelium; st, stroma. C) Immunostaining for FOXO1. FOXO1 was detectable in the nucleolus of uterine epithelial cells at the time of embryo implantation around the peri-implantation site in *Zip10* cKO mice (D). Scale bar: 100 μm. em, embryo; ge, glandular epithelium; le, luminal epithelium; st, stroma.

Decidualization treatment resulted in a change in the localization of GLI1 from the nucleus to the cytoplasm of the cells in the control plasmid vector (Control-sh), whereas cells in which GLI1 remained in the nucleus were observed in Zip10-sh (Fig. 6A, B). Decidual marker gene expression (*PRL* and *IGFBP1*) (43) was significantly upregulated after decidual stimuli in both control-sh and Zip10-sh, although the expression with Zip10-sh was significantly lower than that of the control (Fig. S9). These results suggest that Zip10-mediated uptake of zinc ions into the cytoplasm is important for progesterone signaling not only in mice but also in humans.

Discussion

Our present findings demonstrate that intracellular zinc, regulated by the endometrial zinc transporter ZIP10, is essential for successful embryo implantation and placentation in mice. In particular, the results revealed that an intracellular zinc deficiency due to a lack of ZIP10 impairs the P4 responsiveness of the endometrium, resulting in both the failure of degradation for the luminal epithelium and embryonic loss (Fig. 6C).

In this study, the deletion of ZIP10 by Pgr^{Cre} manifested a phenotype as early as D5 of pregnancy as abnormally sustained PGR expression in the luminal epithelium with a decreased expression of most P4 target genes, although the morphology of the uterine tissues of the *Zip10* cKO and control mice was comparable. The initial reaction of embryo implantation, including embryo apposition and attachment, was not disrupted in the *Zip10* cKO mice, as aligned implantation sites was clearly visualized by blue dye and the number of implantation sites was not decreased in the *Zip10* cKO mice on D5 (Fig. 2B, C, E). This is further confirmed by our observation that only minor differences in gene expression were observed in D4 (Fig. S5, Datasets S1), and the expressions of *Lif* and *Lifr*, which are essential factors for embryo attachment (44), were not significantly different between the *Zip10* cKO and control mice (Fig. 3H). On D6, failure of the embryo implantation process—more specifically failure of embryo invasion—was elicitable, as shown by our finding that embryos were not in direct

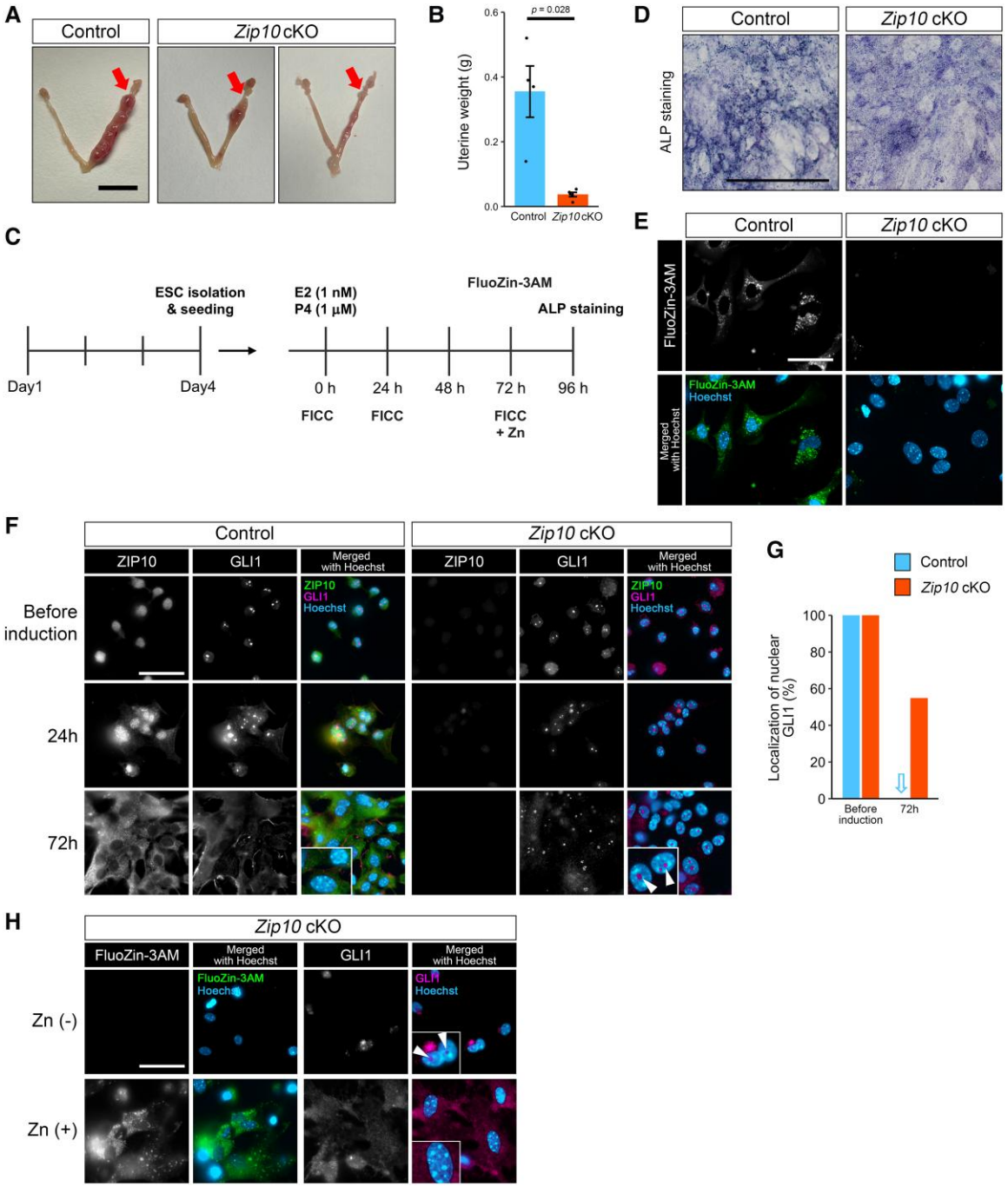

Fig. 5. Intracellular zinc levels and GLI1 localization in decidualizing cells. A) Representative images showing the gross morphology of artificial decidualization (AD) from control and *Zip10* cKO mice. *Red arrows*: the site of sesame oil injection. Scale bar: 1 cm. B) Comparison of uterine weight by AD. C) Experimental procedure for endometrial stromal cell (ESC) isolation and in vitro decidualization. D) Alkaline phosphatase (ALP) staining for decidualized cultured stromal cells. Scale bar: 100 μm. E) Staining with FluoZin-3AM, a zinc ion indicator, in cultured stromal cells. No positive signal for FluoZin-3AM was observed in the cytoplasm of *Zip10* cKO stromal cells. Scale bar: 50 μm. F) Fluorescent immunocytochemistry (FICC) for ZIP10 and GLI1. GLI1 was detected in the cytoplasm of control stromal cells at 72 h but was localized in the nucleus in *Zip10* cKO stromal cells (G) (*arrowheads* in higher magnification inset). Scale bar: 50 μm. H) FluoZin-3AM staining and FICC for GLI1 after chloroquine treatment in *Zip10* cKO stromal cells. Zinc supplementation shifts GLI1 localization from the nucleus (*arrowheads* in higher magnification inset) to the cytoplasm. Scale bar: 50 μm.

contact with stromal cells in the *Zip10* cKO mice (Fig. 3A). This failure was most likely associated with a weak decidualization reaction and subsequent embryonic loss after D6.

Genetic recombination using Pgr^{Cre} may target not only the uterus but also the ovaries and pituitary gland. In fact, it has been reported that *Lgr5* gene deletion by Pgr^{Cre} results in subfertility due to a disruption of P4 production in the corpus luteum (45). The Pgr^{Cre} strain used in our present investigation was based on ires-dependent Cre recombinase expression, which differs from the Pgr^{Cre} strain in that study, but the infertile phenotype may be triggered by a genetic defect in the newly formed corpus luteum (33). In our study, at least, no P4 depletion was observed in the *Zip10* cKO mice during early pregnancy (Fig. 2F). To exclude the possibility that a pituitary–ovarian axis defect caused the

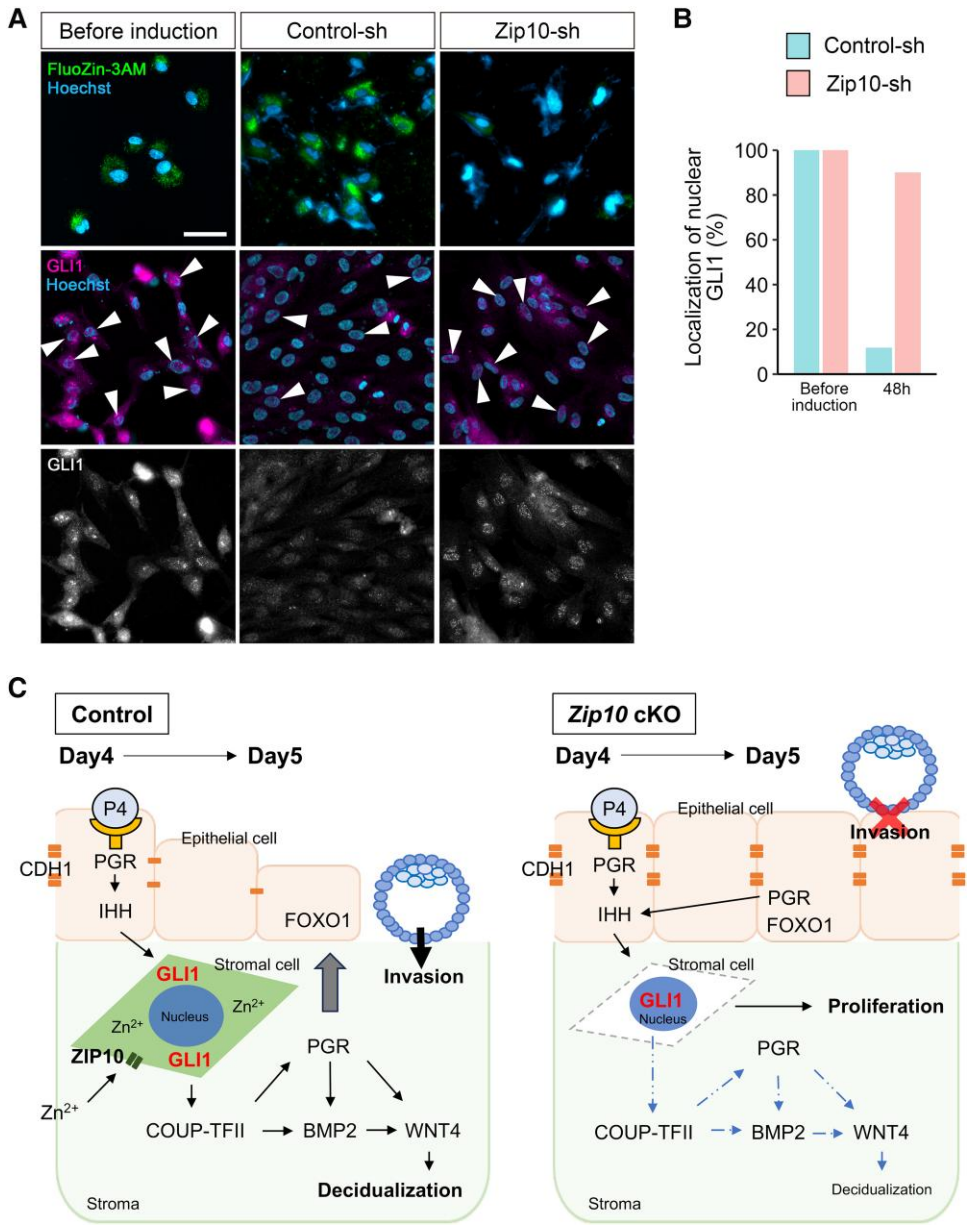

Fig. 6. Zinc dynamics and GLI1 localization in human endometrial cell and model of embryo invasion regulated by ZIP10. A) Transfection of Zip10-sh in human endometrial stromal cells resulted in reduced intracellular FluoZin-3AM signal. Scale bar: 50 μm. Nuclear GLI1 localization (*arrowheads*), shown before decidual induction, was persistent 48 h after decidual stimulation with Zip10-sh (B). C) Model of embryo invasion regulated by zinc dynamics though ZIP10. Zinc ion regulates P4-PGR signaling during embryo implantation. In *Zip10* cKO mice, zinc ion is not incorporated into the uterine cells, leading to the nuclear localization of stromal GLI1 and attenuation of P4-PGR signaling. This results in incomplete decidualization and a failure of the elimination of epithelial cells that allows embryonic invasion, and thus subsequent embryonic loss.

infertile phenotype in the *Zip10* cKO mice, we used a delayed implantation model. In mice, pregnancy can be maintained by the administration of external hormones after the removal of ovaries in the delayed implantation model (46, 47). Our results demonstrated that the imbalance of hormones was not the main cause of pregnancy failure in the *Zip10* cKO mice. The E2 levels were 1,000 times lower than those of P4, which may have resulted in the differences in variation among the individual mice.

We also observed that the deletion of ZIP10 in the endometrium, especially in stromal cells, was not directly linked to the functional loss for decidualization, because a weak decidualization reaction was observed in the *Zip10* cKO uteri (Fig. 2E) and the partial deciduoma could be induced after an intrauterine oil infusion with decidual marker gene expression (Fig. 5A, Fig. S8). Furthermore, after the in vitro induction of decidualization, isolated stromal cells from *Zip10* cKO mice exhibited ALP activity, which is a well-known marker of stromal differentiation (37) (Fig. 5C, D). The results from human endometrial stromal cells may support our idea. Our results indicates that the cause of the pregnancy failure observed in the *Zip10* cKO mice is most likely due to a failure of epithelial–stromal interaction during early pregnancy.

The prereceptive mouse uterus (D1 to D3) is under an E2-dominant state, with proliferation of epithelial cells (48). P4 signal, mediated by both epithelial and stromal PGR, counteracts E2, and it is required for implantation of embryos in the receptive uterus (49). IHH, a secreted morphogen, is transiently expressed in the preimplantation uterine epithelium by P4-PGR (38, 50), and

its expression is also reported to be enhanced by LIF stimulation (51). Secreted IHH from the uterine epithelium binds to the canonical IHH receptor PTCH1 in the underlying stroma, resulting in the de-repression of SMO and the activation of GLI, which is a zinc-finger transcription factor.

Activation of the IHH pathway leads to a promotion of the expression of COUP-TFII (also known as NR2F2), which subsequently upregulates the stromal PGR expression and induces BMP2, WNT4, and HAND2, which are essential factors for decidualization (49). HAND2 is also a stromal P4-PGR target transcription factor that normally inhibits the expression of several members of the fibroblast growth factor (FGF) family that promotes uterine epithelium proliferation (34, 49). HOXA10 is another stromal P4-PGR target transcription factor involved in decidualization (52). In the present study, the expressions of these P4-PGR target genes were disrupted; most of them were downregulated, with the exception of *Ihh* (Fig. 4). Increased expression of *Ihh* is closely related to the sustained PGR expression in the luminal epithelium. Under normal conditions, PGR expression shifts from the uterine epithelium to the uterine stroma in the progression of the embryo implantation process (53).

Wetendorf et al. reported that a constitutive expression of PGR in the luminal epithelium of transgenic strains resulted in the failure of embryo attachment, and it was concluded that a loss of epithelial PGR expression is necessary for successful embryo implantation (54). The expressions of *Lif* and *Lifr* were significantly reduced in that mouse model, which is not in agreement with our *Zip10* cKO findings. Our present results support their conclusion more precisely: a constitutive expression of epithelial PGR inhibits the detachment of the luminal epithelium. The absence of *Hand2* in uterine tissues was described in a study of embryo implantation failure due to the persistent proliferation of uterine epithelial cells during early pregnancy (34). In *Zip10* cKO mice, epithelial cell proliferation had ceased at the timing of embryo implantation (Fig. 3B), suggesting that (at least) the stromal P4-PGR signal that regulates epithelial cell proliferation, such as the FGF–FGF receptor axis (FGFR) (49) is likely unimpaired. In contrast, cell proliferation of the subluminal stromal region was enhanced in *Zip10* cKO mice (Fig. 3B, C), suggesting that stromal cells progressed in the direction of proliferation rather than differentiation.

Despite the higher expression of *Ihh* in *Zip10* cKO mice, we observed that downstream targets of the stromal P4-PGR axis were substantially decreased. We suggest that an epithelial–stromal signal interaction exists to control the epithelial P4-PGR signal. FOXO1, a member of the forkhead transcription factor family, was reported to regulate the epithelial PGR expression (40). Ablation of uterine FOXO1 expression led to the PGR expression being retained in the uterine epithelium during the window of receptivity, which resulted in infertility (40). In the present study, the FOXO1 expression in the *Zip10* cKO group did not disappear during embryo implantation, indicating that other factors may be involved in the regulation of PGR expression. FOXO1 expression persisted in the nuclei of implanted peri-embryonic epithelia in *Zip10* cKO mice, unlike the control (Fig. 4C, D). Therefore, it remains possible that the lack of ZIP10 affects the functional loss of FOXO1.

Epas1, also called hypoxia-inducible factor 2α (*Hif2α*), regulates embryo invasion through basement-membrane remodeling and the degradation of the luminal epithelium, since a uterine- and stromal-deletion of *Hif2α* resulted in implantation failure and pregnancy loss (41, 42). Since *Epas1* expression was not altered in *Zip10* cKO uteri (Fig. S7), the loss of *Zip10* in the stroma is not directly linked to the loss of HIF. Our present findings demonstrated that the localization of intracellular GLI1 was highly affected by the intracellular zinc depletion caused by ZIP10 loss in the cultured uterine stromal cells (Fig. 5E-H). GLI1 is a member of the Kruppel family of zinc-finger proteins, which are stabilized by zinc ion (55). Nucleocytoplamic shuttling of the GLI protein is closely linked to the signaling on and off of the Hedgehog signaling pathway (56, 57). It may be important to note that GLI localizes to the nucleus of the cell and activates downstream target genes by decidual stimuli, but is then transported to the cytoplasm. Since the subluminal stromal cells in *Zip10* cKO are highly proliferative (Fig. 3B, C), GLI localization may impact on the switch between cell differentiation or cell proliferation. We also found that the nuclear-cytoplasmic localization of GLI1 is altered in human endometrial stromal cells upon decidual stimulation in vitro (Fig. 6), indicating that intracytoplasmic zinc depletion can affect the localization of GLI1. It would be interesting to investigate the relationship between the function(s) of GLI1 and zinc depletion.

In conclusion, we have shown that uterine ZIP10, which functions as an influx of zinc ions into the intracellular space, is essential for successful embryo implantation and placentation in mice. Zinc signal plays an important role in the P4-PGR signal that helps embryo invasion into the endometrium. Zinc deficiency has been a problem in developing countries, but is also present in developed countries where adequate nutrition is available (58). A correlation between serum zinc concentrations and birth weight and pregnancy outcomes has been suggested (58, 59). Our results highlight an essential zinc-related molecular mechanism to support the establishment and maintenance of pregnancy.

Materials and methods

All chemicals and reagents were purchased from Sigma-Aldrich (St. Louis, MO, USA) unless otherwise stated. All animal procedures were approved by the Ethical Committee for Vertebrate Experiments at Azabu University (ID#200312-24). All experiments were conducted in accord with the relevant guidelines and regulations, including the Animal Research: Reporting of In Vivo Experiments (ARRIVE) guidelines.

Animals

The mice were housed in the barrier facility at Azabu University. The following mouse strains were used: $Pgr^{Cre/+}$ mouse < B6.129S(Cg)-$Pgr^{tm1.1(cre)Shah}$/AndJ, JAX: 017915> (32) and *Slc39a10/Zip10*$^{flox/flox}$ (*Zip10*$^{f/f}$) mouse < $Slc39a10^{tm1.1Tfk}$ > (60). All strains were maintained on the C57BL/6J background purchased from Jackson Laboratory Japan (Kanagawa, Japan). All mice were fed ad libitum under a 12-h light/12-h dark photocycle at 23 ± 2 °C.

Uterine-specific *Slc39a10/Zip10*-deficient (*Zip10* conditional knockout [cKO]) mice were generated by several crossings of the $Pgr^{Cre/+}$ strain with the *Zip10*$^{flox/flox}$ strain (Fig. S1). The genotype of the mice was confirmed by the polymerase chain reaction (PCR) of genomic DNA obtained from tail tissue (Fig. S1A).

The PCR primers used for genotyping were 5′-AGTTATTG CTGCCCAGTTGC-3′, 5′-CCCTTTCTCATGGAGATCTGTC-3′, and 5′-GCGCTAAGGATGACTCTGGTC-3′ for Pgr^{Cre}; and 5′-CAAGGC CAGCCAAAATTCTA-3′, 5′-GCTTTCCTCCCATCCTGATT-3′, and 5′-GTGGCATGCGTGGAAGTTAG-3′ for *Zip10*^{flox}. Sexually mature (> 8 weeks old) $Pgr^{Cre/+}$; *Zip10*$^{flox/flox}$ and $Pgr^{Cre/+}$; *Zip10*$^{flox/-}$ female mice were used as *Zip10* cKO mice. $Pgr^{+/+}$; *Zip10*$^{flox/flox}$ and $Pgr^{+/+}$; *Zip10*$^{flox/-}$ females were used as the control mice, since unexpected germline recombination was sometimes identified in $Pgr^{Cre/+}$ lines as reported (33) (Fig. S1B).

Females were mated with a fertile wildtype male. The day when the vaginal plug was first observed was designated as the first day of pregnancy (D1). Mice were euthanized by cervical dislocation after a combination anesthetic with 0.75 mg/kg of medetomidine, 4.0 mg/kg of midazolam, and 5.0 mg/kg of butorphanol at indicated day(s) of pregnancy (61). Uterine and ovarian tissues harvested at indicated day(s) of pregnancy were fixed with 4% paraformaldehyde (PFA) solution in phosphate-buffered saline (PBS) for histological study, fixed with G-Fix (Genostaff, Tokyo, Japan) for in situ hybridization (ISH) and snap-frozen and kept at −80 °C until used for RNA extraction.

The implantation sites were visualized by an intravenous injection of 0.1 mL of 1% Chicago blue dye dissolved in saline as described (62). After female mice were mated with a vasectomized male, artificial decidualization was performed by the administration of intraluminal injections of 0.02 mL of sesame oil as described (63).

In order to control the embryo implantation process by an administration of exogenous hormone, the ovaries of control and *Zip10* cKO females were removed at D4, followed by the insertion of a Silactic implant (20 mm long × 2.0 mm inner dia., 3.0 mm outer dia., Silascon 100-2N, Kaneka Medix, Osaka, Japan) containing progesterone (P4) powder under the dorsal skin (Fig. S3A). Two days later, a single subcutaneous injection of 17β-estradiol (E2, 25 ng/head) was performed to induce embryo implantation. Uterine tissues were collected 3 days after the E2 injection to verify successful embryo implantation and decidualization.

Measurement of serum hormone levels

Blood samples from indicated mice were collected through cardiac puncture under combination anesthetic on D5, 6, 8, and 10 of pregnancy. Serum was separated by centrifugation (4 °C, 7,000×g, 7 min) and stored at −80 °C until analysis. The serum concentrations of P4 and E2 were measured by enzyme-linked immunosorbent assays as described (64).

Histology

Fixed uterine and ovarian tissues were paraffin-embedded, and the paraffin sections (6 µm) were stained with hematoxylin and eosin (H&E).

In situ hybridization

In situ hybridization was performed as described with some modifications (60). Briefly, fixed uterine tissues were paraffin-embedded, and the paraffin sections (6 µm) were mounted on MAS-coated slides (Matsunami Glass Industries, Osaka, Japan) under RNase-free conditions. Sense or antisense digoxigenin (DIG)-labeled RNA probes for *Slc39a10*/*Zip10* were purchased from Genostaff. The sections were deparaffinized, rehydrated, and post-fixed in 10% neutral buffered formalin (NBF) for 30 min at 37 °C, followed by treatment with 0.2% hydrogen chloride and 5 µg/mL proteinase K (FujiFilm Wako Pure Chemicals, Osaka, Japan) for 10 min at 37 °C, respectively. Hybridization was performed with DIG-labeled probes (300 ng/300 µL/slide) in a humidified chamber at 60 °C overnight.

The slides were washed after hybridization, then treated with blocking reagent (Genostaff) for 15 min and with alkaline phosphatase (ALP)-conjugated anti-DIG antibody (1:2,000; Roche Diagnostics, Basel, Switzerland) for 1 h at RT. The signals were detected by 4-nitro-blue tetrazolium/5-bromo-4-chloro-3-indolyl phosphate (NBT/BCIP, Roche Diagnostics) in a humidified container for 72 h at 4 °C. The sections were counterstained with Kernechtrot solution (Muto Pure Chemicals, Tokyo, Japan). Signals detected by the sense probe were used as a control for background levels.

Immunohistochemistry and immunofluorescence

Fixed tissues were paraffin-embedded, and the paraffin sections (6 µm) were deparaffinized, hydrated, and used for antigen retrieval by autoclaving in 10 mM sodium citrate buffer (pH = 6.0) for 5 min. For immunohistochemistry (IHC), the sections were further incubated in 3% hydrogen peroxide diluted with methanol for 15 min. After blocking with a nonspecific staining blocking reagent (X0909, Dako, Carpinteria, CA, USA), the slides were incubated with primary antibodies (shown in Table S1) overnight at 4 °C. The same slides were subjected to incubation with the Histofine mouse stain kit (Nichirei Biosciences, Tokyo, Japan) for 1 h. Signals were visualized by 3,3′-diaminobenzidine tetrahydrochloride and counterstained with hematoxylin.

For the immunofluorescence (IF) evaluation, the slides were incubated with Alexa Fluor 488-conjugated secondary antibodies (Jackson Immuno Research Laboratories, West Grove, PA) for 1 h, and mounted with ProLong Glass Antifade Mountant with NucBlue Stain (P36981, Thermo Fisher Scientific, Waltham, MA, USA). Micrographs were captured by PROVIS AX80 microscopy (Olympus, Tokyo) or BZ-X700 microscopy (Keyence, Osaka, Japan). All signals were detected under the same lighting conditions for the control and *Zip10* cKO groups. The number of immunostain-positive cells was counted >1,000 for MKI67 and >100 for PGR using Image J (65) ($n \geq 3$); for FOXO1, the number of epithelial cells (93.8 ± 8.0, mean ± SD) at the same distance around the embryo was evaluated in control and *Zip10* cKO ($n \geq 3$).

Western blotting

Whole uterine tissues on D6 were lysed in Ripa buffer and diluted with the Laemmli sample buffer (Bio-Rad Laboratories, Hercules, CA, USA) containing 5% 2-mercaptoethanol. Samples (20 µg total protein) were separated on 8% Bis-Tris gels using sodium dodecyl sulfate-polyacrylamide gel electrophoresis and transferred to PVDF membranes (Bio-Rad Laboratories). The PVDF membranes were blocked in 10% skim milk (FujiFilm Wako Pure Chemicals) in Tris-buffered saline with 0.1% Tween-20 and probed overnight with primary antibody at 4 °C. The membranes were incubated with the secondary antibody, horseradish peroxidase-conjugated anti-rabbit, or anti-mouse IgG (1:5,000; Cell Signaling Technology, Danvers, MA, USA) for 1 h at RT. After the membranes were washed, the immunoreactive proteins were visualized using the ECL Western Blotting Analysis System (Cytiva, Tokyo, Japan) according to the manufacturer's recommendations. Signals were captured using an ImageQuant LAS 4000 (Cytiva).

RNA extraction and quantitative PCR

Total RNA was isolated using the RNeasy Plus Mini kit (Qiagen, Venlo, Netherlands) according to the manufacturer's instructions. After the total RNA concentration was measured using a Nanodrop system (ND-1000, Thermo Fisher Scientific), 1 µg of total RNA in each sample was reverse-transcribed with SuperScript III or IV Reverse Transcriptase (#18080-044 or #18090-050, Thermo Fisher Scientific) using oligo-dT primer (#3805, Takara, Shiga, Japan). A quantitative (q)PCR was performed on a Thermal Cycler Dice Real Time System (Takara) with the use of Power SYBR Green Master Mix (A25742, Thermo Fisher Scientific) or KAPA SYBR Fast qPCR Kit (KK4601, NIPPON Genetics, Tokyo,

Japan). The primer sequences used in this study are shown in Table S2 for mouse and S3 for human. The relative expression values of the target transcripts were evaluated using the ΔΔCt relative quantification method (66) with normalization to *Gapdh* (*GAPDH*). The average values of control samples were set as 1.0.

RNA sequencing

RNA-seq was carried out by Azenta Life Sciences (Burlington, MA, USA). Briefly, 1 μg total RNA isolated using the RNeasy Plus Mini kit was used for following library preparation. The poly(A) mRNA isolation was performed using Oligo(dT) beads. The mRNA fragmentation was performed using divalent cations and high temperature. Priming was performed using Random Primers. First-strand cDNA and the second-strand cDNA were synthesized. The purified double-stranded cDNA was then treated to repair both ends and add a dA-tailing in one reaction, followed by a T-A ligation to add adaptors to both ends. Size selection of Adaptor-ligated DNA was then performed using DNA Clean Beads. Each sample was then amplified by PCR using P5 and P7 primers and the PCR products were validated. Then libraries with different indexes were multiplexed and loaded on an MGI2000 instrument for sequencing using a 2 × 150 paired-end (PE) configuration according to manufacturer's instructions. The FASTQ files were processed for removal of adaptor sequences, trimmed, and quality-based filtered using fastp v0.23.2 (67). The trimmed reads were removed ribosomal RNA using SortMeRNA v4.3.6 (68). The removed reads were mapped onto the reference genome of *Mus musculus* (GRCm39) using STAR v2.7.10a (69). Mapped reads were counted using RSEM v1.3.3 (70). Differential expression analysis was performed in R v4.2.1 (https://www.R-project.org/.) using the EdgeR v 3.38.4 package (71) and visualized significantly different genes as MA-plot and heatmap using the gplots v3.1.3 and genefilter v1.78.0 packages.

Isolation and culture of primary uterine stromal cells

For the isolation and culture of primary uterine stromal cells, uterine stromal cell isolation and culture were performed as described with minor modifications (37). Briefly, uterine horns collected on day 4 of pregnancy were rinsed with phenol red-free Hank's balanced salt solution (HBSS)(−) (#085-09355, FujiFilm Wako Pure Chemicals) containing 1× antibiotic–antimycotic solution (#161-23181, FujiFilm Wako Pure Chemicals) for the removal of blood and trimmed fat and mesometrial tissues. Uterine tissues were cut into 3- to 4-mm lengths with sterile scissors and incubated in phenol red-free HBSS(−) containing dispase (#17105-041, Thermo Fisher Scientific) and pancreatin (#P3292) at 4 °C for 1 h, followed by incubation at RT for 1 h and at 37.5 °C for 10 min. The enzyme reaction was stopped by the addition of fetal bovine serum (FBS) (Biowest, Nuaillé, France).

Uterine pieces were washed with phenol red-free free HBSS(−) to remove epithelial cells and further incubated in phenol red-free free HBSS(−) with collagenase type III (#CLS3, Worthington, Lakewood, NJ) at 37.5 °C for 30 min. After the addition of FBS, the uterine pieces were washed with phenol red-free free HBSS(−) and passed through a 70-μm cell strainer (Corning, Glendale, AZ, USA). Isolated uterine stromal cells were concentrated by centrifugation (900×g, 7 min), inoculated into 35-mm glass-bottomed dishes (Matsunami Glass Industries), and incubated with D-MEM/Ham's F-12 culture medium (#045-30665, FujiFilm Wako Pure Chemicals) containing 10% charcoal-stripped FBS (CS-FBS) (Cytiva) and 1× penicillin/streptomycin solution (#168-23191, FujiFilm Wako Pure Chemicals) at 37.5 °C under 5% CO_2. The culture medium was changed 1 h after inoculation, and adherent cells were continuously incubated for 24 h.

For the induction of in vitro decidualization, the medium was replaced with D-MEM/Ham's F-12 containing 2% CS-FBS, 1 nM E2, and 1 μM P4. ALP staining with BCIP/NBT Color Development Substrate solution (#S3771, Promega, Madison, WI, USA) was performed to detect the successful decidual reaction as described (72, 73). Detection of intracellular zinc levels was observed after 60 min of incubation in Opti-MEM (Thermo Fisher Scientific) supplemented with 1 μM of FluoZin-3AM (Thermo Fisher Scientific). For the zinc supplementation, cultured stromal cells were incubated with Opti-MEM with 1% dimethyl sulfoxide (DMSO) containing 5 μM $ZnCl_2$ (#260-00272, FujiFilm Wako Pure Chemicals) and 300 μM chloroquine for 30 min before collection (74). Fluorescent immunocytochemistry (FICC) was performed on fixed cells collected at the indicated times after the medium replacement.

Human endometrial stromal cell culture

The immortalized human endometrial stromal cell line (43) was cultured in D-MEM/Ham's F-12 culture medium containing 10% CS-FBS (Cytiva) and 1× penicillin/streptomycin/neomycin mixture (#15640055, Thermo Fisher Scientific) at 37.5 °C under 5% CO_2. Cell were inoculated into 24-well plates and glass-bottom dishes (D11131H, Matsunami Glass Industries), and shRNA expression vector plasmid (pGFP-V-RS, OriGene Technologies, Rockville, MD, USA) (target sequences are shown in Table S4) was induced with Lipofectamine 3,000 (Thermo Fisher Scientific) according to the manufacturer's recommendations. pCAG-EGFP was used to determine transfection efficiency, and a solution containing 3% Lipofectamine 3,000 reagent showed the highest efficiency. For the induction of in vitro decidualization, the medium was replaced with D-MEM/Ham's F-12 containing 2% CS-FBS, 0.5 mM dibutyryl-cAMP (#330-00731, FujiFilm Wako Pure Chemicals), and 1 μM P4 24 h after plasmid transfection. Cells were harvested before artificial decidualization stimuli and 48 h after treatment. Among the four Zip10-sh plasmids, Zip10-shD caused the most pronounced attenuation of the FluoZin-3AM signal. Therefore, we designated this plasmid as Zip10-sh and confirmed the localization of GLI1 and decidual marker gene expression.

Statistical analysis

All of the data are presented as the mean ± standard error of mean (SEM). Differences in the data were examined with the use of Student's t test or the Mann–Whitney *U* test. One-way ANOVA was used for multiple samples. A p-value <0.05 was considered significant.

Acknowledgments

We thank members of the Laboratory of Animal Reproduction for technical help. We also thank RIKEN BRC for providing $Zip10^{flox}$ mice, and Dr. FC. Yang (University of California) for providing Pgr^{Cre} mice. We also thank Dr. M. Yoshie and Dr. K. Tamura (Tokyo University of Pharmacy and Life Sciences) for providing an immortalized human endometrial stromal cell line.

Supplementary Material

Supplementary material is available at *PNAS Nexus* online.

Funding

This work was partially supported by JSPS KAKENHI Grant Numbers JP21K09512 (to J.T.), JP21H02384 and JP20H05373 (to J.I.), and JP21K05977 (to N.K.). This study was also supported by the Supported Program for the Private University Research Branding Project (2016–2019) from Japan's Ministry of Education, Culture, Sports, Science and Technology. This research was partially supported by the Center for Human and Animal Symbiosis Science, Azabu University and a research project grant awarded by the Azabu University Research Services Division.

Author Contributions

Conceptualization: Y.K. and J.I.; resources: T.F.; data curation, Y.K., J.T., and J.I.; formal analysis: H.M.; supervision: J.I. and N.K.; funding acquisition: J.T., J.I., and N.K.; validation: Y.K., A.T. and T.N.; investigation: Y.K., J.T., A.T., T.N., A.K., M.N., and H.M.; visualization: Y.K., J.T., and J.I.; methodology: J.T., M.N., H.M., T.F., J.I., and N.K.; writing—original draft: Y.K., J.T., and J.I.; project administration: Y.K., J.T., and J.I.; writing—review & editing: Y.K., J.T., Y.F., J.I., and N.K.

Preprint

This manuscript was posted on a preprint: https://doi.org/10.1101/2023.09.26.559476.

Data Availability

The datasets generated and/or analyzed during the current study are available in the GEO repository, accession number GSE252322.

References

1 Zegers-Hochschild F, *et al.* 2017. The international glossary on infertility and fertility care, 2017. *Fertil Steril*. 108:393–406.
2 Inhorn MC, Patrizio P. 2015. Infertility around the globe: new thinking on gender, reproductive technologies and global movements in the 21st century. *Hum Reprod Update*. 21:411–426.
3 Skoracka K, Ratajczak AE, Rychter AM, Dobrowolska A, Krela-Kaźmierczak I. 2021. Female fertility and the nutritional approach: the most essential aspects. *Adv Nutr*. 12:2372–2386.
4 Barker M, *et al.* 2018. Intervention strategies to improve nutrition and health behaviours before conception. *Lancet*. 391:1853–1864.
5 Ebisch IMW, Thomas CMG, Peters WHM, Braat DDM, Steegers-Theunissen RPM. 2007. The importance of folate, zinc and antioxidants in the pathogenesis and prevention of subfertility. *Hum Reprod Update*. 13:163–174.
6 Saper RB, Rash R. 2009. Zinc: an essential micronutrient. *Am Fam Physician*. 79:768–772.
7 Rink L, Gabriel P. 2000. Zinc and the immune system. *Proc Nutr Soc*. 59:541–552.
8 Maret W, Sandstead HH. 2006. Zinc requirements and the risks and benefits of zinc supplementation. *J Trace Elem Med Biol*. 20:3–18.
9 Prasad AS. 1998. Zinc and immunity. *Mol Cell Biochem*. 188:63–69.
10 Prasad AS. 2001. Recognition of zinc-deficiency syndrome. *Nutrition*. 17:67–69.
11 Caulfield LE, Zavaleta N, Shankar AH, Merialdi M. 1998. Potential contribution of maternal zinc supplementation during pregnancy to maternal and child survival. *Am J Clin Nutr*. 68:499S–508S.
12 Ota E, *et al.* 2015. Zinc supplementation for improving pregnancy and infant outcome. *Cochrane Database Syst Rev*. 2015:CD000230.
13 Khadem N, *et al.* 2012. Relationship between low birth weight neonate and maternal serum zinc concentration. *Iran Red Crescent Med J*. 14:240–244.
14 Prasad AS. 1985. Clinical, endocrinologic, and biochemical effects of zinc deficiency. *Spec Top Endocrinol Metab*. 7:45–76.
15 Castillo-Durán C, Weisstaub G. 2003. Zinc supplementation and growth of the fetus and low birth weight infant. *J Nutr*. 133:1494S–1497S.
16 Tian X, Anthony K, Neuberger T, Diaz FJ. 2014. Preconception zinc deficiency disrupts postimplantation fetal and placental development in mice. *Biol Reprod*. 90:83.
17 Wilson RL, *et al.* 2017. Zinc is a critical regulator of placental morphogenesis and maternal hemodynamics during pregnancy in mice. *Sci Rep*. 7:15137.
18 Kambe T, Tsuji T, Hashimoto A, Itsumura N. 2015. The physiological, biochemical, and molecular roles of zinc transporters in zinc homeostasis and metabolism. *Physiol Rev*. 95:749–784.
19 Hirano T, *et al.* 2008. Roles of zinc and zinc signaling in immunity: zinc as an intracellular signaling molecule. *Adv Immunol*. 97:149–176.
20 Kambe T, Yamaguchi-Iwai Y, Sasaki R, Nagao M. 2004. Overview of mammalian zinc transporters. *Cell Mol Life Sci*. 61:49–68.
21 Fukada T, Kambe T. 2011. Molecular and genetic features of zinc transporters in physiology and pathogenesis. *Metallomics*. 3:662–674.
22 Palmiter RD, Huang L. 2004. Efflux and compartmentalization of zinc by members of the SLC30 family of solute carriers. *Pflugers Arch*. 447:744–751.
23 Eide DJ. 2004. The SLC39 family of metal ion transporters. *Pflugers Arch*. 447:796–800.
24 Fukada T, Yamasaki S, Nishida K, Murakami M, Hirano T. 2011. Zinc homeostasis and signaling in health and diseases: zinc signaling. *J Biol Inorg Chem*. 16:1123–1134.
25 Baltaci AK, Yuce K. 2018. Zinc transporter proteins. *Neurochem Res*. 43:517–530.
26 Grzeszczak K, Kwiatkowski S, Kosik-Bogacka D. 2020. The role of Fe, Zn, and Cu in pregnancy. *Biomolecules*. 10:1176.
27 Schmitt-Ulms G, Ehsani S, Watts JC, Westaway D, Wille H. 2009. Evolutionary descent of prion genes from the ZIP family of metal ion transporters. *PLoS One*. 4:e7208.
28 Miyai T, *et al.* 2014. Zinc transporter SLC39A10/ZIP10 facilitates antiapoptotic signaling during early B-cell development. *Proc Natl Acad Sci U S A*. 111:11780–11785.
29 Hobeika E, *et al.* 2006. Testing gene function early in the B cell lineage in mb1-cre mice. *Proc Natl Acad Sci U S A*. 103:13789–13794.
30 He X, *et al.* 2023. The zinc transporter SLC39A10 plays an essential role in embryonic hematopoiesis. *Adv Sci (Weinh)*. 10:e2205345.
31 Wu C, *et al.* 2009. BioGPS: an extensible and customizable portal for querying and organizing gene annotation resources. *Genome Biol*. 10:R130.
32 Yang CF, *et al.* 2013. Sexually dimorphic neurons in the ventromedial hypothalamus govern mating in both sexes and aggression in males. *Cell*. 153:896–909.
33 Namiki T, *et al.* 2021. Utility of progesterone receptor-ires-Cre to generate conditional knockout mice for uterine study. *Anim Sci J*. 92:e13615.
34 Li Q, *et al.* 2011. The antiproliferative action of progesterone in uterine epithelium is mediated by Hand2. *Science*. 331:912–916.

35 Namiki T, *et al.* 2023. Uterine epithelial Gp130 orchestrates hormone response and epithelial remodeling for successful embryo attachment in mice. *Sci Rep*. 13:854.

36 Lim H, Ma L, Ma WG, Maas RL, Dey SK. 1999. Hoxa-10 regulates uterine stromal cell responsiveness to progesterone during implantation and decidualization in the mouse. *Mol Endocrinol*. 13: 1005–1017.

37 Li Q, *et al.* 2007. Bone morphogenetic protein 2 functions via a conserved signaling pathway involving Wnt4 to regulate uterine decidualization in the mouse and the human. *J Biol Chem*. 282: 31725–31732.

38 Takamoto N, Zhao B, Tsai SY, DeMayo FJ. 2002. Identification of Indian hedgehog as a progesterone-responsive gene in the murine uterus. *Mol Endocrinol*. 16:2338–2348.

39 Franco HL, *et al.* 2010. Constitutive activation of smoothened leads to female infertility and altered uterine differentiation in the mouse. *Biol Reprod*. 82:991–999.

40 Vasquez YM, *et al.* 2018. FOXO1 regulates uterine epithelial integrity and progesterone receptor expression critical for embryo implantation. *PLoS Genet*. 14:e1007787.

41 Matsumoto L, *et al.* 2018. HIF2α in the uterine stroma permits embryo invasion and luminal epithelium detachment. *J Clin Invest*. 128:3186–3197.

42 Bhurke A, *et al.* 2020. A hypoxia-induced Rab pathway regulates embryo implantation by controlled trafficking of secretory granules. *Proc Natl Acad Sci U S A*. 117:14532–14542.

43 Tamura K, Yoshie M, Hara T, Isaka K, Kogo H. 2007. Involvement of stathmin in proliferation and differentiation of immortalized human endometrial stromal cells. *J Reprod Dev*. 53:525–533.

44 Cha J, Sun X, Dey SK. 2012. Mechanisms of implantation: strategies for successful pregnancy. *Nat Med*. 18:1754–1767.

45 Sun X, *et al.* 2014. Ovarian LGR5 is critical for successful pregnancy. *FASEB J*. 28:2380–2389.

46 Milligan SR, Finn CA. 1997. Minimal progesterone support required for the maintenance of pregnancy in mice. *Hum Reprod*. 12:602–607.

47 Terakawa J, *et al.* 2012. The complete control of murine pregnancy from embryo implantation to parturition. *Reproduction*. 143:411–415.

48 Namiki T, Ito J, Kashiwazaki N. 2018. Molecular mechanisms of embryonic implantation in mammals: lessons from the gene manipulation of mice. *Reprod Med Biol*. 17:331–342.

49 DeMayo FJ, Lydon JP. 2020. 90 YEARS OF PROGESTERONE: new insights into progesterone receptor signaling in the endometrium required for embryo implantation. *J Mol Endocrinol*. 65:T1–T14.

50 Matsumoto H, Zhao X, Das SK, Hogan BLM, Dey SK. 2002. Indian hedgehog as a progesterone-responsive factor mediating epithelial-mesenchymal interactions in the mouse uterus. *Dev Biol*. 245:280–290.

51 Wakitani S, Hondo E, Phichitraslip T, Stewart CL, Kiso Y. 2008. Upregulation of Indian hedgehog gene in the uterine epithelium by leukemia inhibitory factor during mouse implantation. *J Reprod Dev*. 54:113–116.

52 Marquardt RM, Kim TH, Shin J-H, Jeong J-W. 2019. Progesterone and estrogen signaling in the endometrium: what goes wrong in endometriosis? *Int J Mol Sci*. 20:3822.

53 Kobayashi R, *et al.* 2017. The window of implantation is closed by estrogen via insulin-like growth factor 1 pathway. *J Reprod Infertil*. 18:231–241.

54 Wetendorf M, *et al.* 2017. Decreased epithelial progesterone receptor A at the window of receptivity is required for preparation of the endometrium for embryo attachment. *Biol Reprod*. 96: 313–326.

55 Kinzler KW, Ruppert JM, Bigner SH, Vogelstein B. 1988. The GLI gene is a member of the Kruppel family of zinc finger proteins. *Nature*. 332:371–374.

56 Hatayama M, Aruga J. 2012. Gli protein nuclear localization signal. *Vitam Horm*. 88:73–89.

57 Kroft TL, *et al.* 2001. GLI1 localization in the germinal epithelial cells alternates between cytoplasm and nucleus: upregulation in transgenic mice blocks spermatogenesis in pachytene. *Biol Reprod*. 65:1663–1671.

58 Wilson RL, Grieger JA, Bianco-Miotto T, Roberts CT. 2016. Association between maternal zinc status, dietary zinc intake and pregnancy complications: a systematic review. *Nutrients*. 8: 641.

59 Neggers YH, *et al.* 1990. A positive association between maternal serum zinc concentration and birth weight. *Am J Clin Nutr*. 51: 678–684.

60 Bin B-H, *et al.* 2017. Requirement of zinc transporter ZIP10 for epidermal development: implication of the ZIP10-p63 axis in epithelial homeostasis. *Proc Natl Acad Sci U S A*. 114:12243–12248.

61 Kawai S, Takagi Y, Kaneko S, Kurosawa T. 2011. Effect of three types of mixed anesthetic agents alternate to ketamine in mice. *Exp Anim*. 60:481–487.

62 Kelleher AM, *et al.* 2017. Forkhead box a2 (FOXA2) is essential for uterine function and fertility. *Proc Natl Acad Sci U S A*. 114: E1018–E1026.

63 Tranguch S, Chakrabarty A, Guo Y, Wang H, Dey SK. 2007. Maternal pentraxin 3 deficiency compromises implantation in mice. *Biol Reprod*. 77:425–432.

64 Noguchi M, Suzuki T, Sato R, Sasaki Y, Kaneko K. 2020. Artificial lactation by exogenous hormone treatment in non-pregnant sows. *J Reprod Dev*. 66:453–458.

65 Schneider CA, Rasband WS, Eliceiri KW. 2012. NIH image to ImageJ: 25 years of image analysis. *Nat Methods*. 9:671–675.

66 Livak KJ, Schmittgen TD. 2001. Analysis of relative gene expression data using real-time quantitative PCR and the 2(-Delta Delta C(T)) method. *Methods*. 25:402–408.

67 Chen S, Zhou Y, Chen Y, Gu J. 2018. Fastp: an ultra-fast all-in-one FASTQ preprocessor. *Bioinformatics*. 34:i884–i890.

68 Kopylova E, Noé L, Touzet H. 2012. SortMeRNA: fast and accurate filtering of ribosomal RNAs in metatranscriptomic data. *Bioinformatics*. 28:3211–3217.

69 Dobin A, *et al.* 2013. STAR: ultrafast universal RNA-seq aligner. *Bioinformatics*. 29:15–21.

70 Li B, Dewey CN. 2011. RSEM: accurate transcript quantification from RNA-Seq data with or without a reference genome. *BMC Bioinformatics*. 12:323.

71 Robinson MD, McCarthy DJ, K G. 2010. Smyth, edgeR: a bioconductor package for differential expression analysis of digital gene expression data. *Bioinformatics*. 26: 139–140.

72 Chen L, Belton RJ, Nowak RA. 2009. Basigin-mediated gene expression changes in mouse uterine stromal cells during implantation. *Endocrinology*. 150:966–976.

73 Franco HL, *et al.* 2011. WNT4 is a key regulator of normal postnatal uterine development and progesterone signaling during embryo implantation and decidualization in the mouse. *FASEB J*. 25:1176–1187.

74 Xue J, *et al.* 2014. Chloroquine is a zinc ionophore. *PLoS One*. 9: e109180.